Catalysis Science & Technology

Accepted Manuscript

ROYAL SOCIETY OF CHEMISTRY

www.rsc.org/catalysis

Template-free synthesis of porous carbonaceous solid acids with controllable acid sites and excellent activity for catalyzing synthesis of biofules and fine chemicals

Fujian Liu*[a], Bojie Li[b], Chen Liu[a], Weiping Kong[a], Xianfeng Yi[c], Anmin Zheng*[c], Chenze Qi*[a]

[a] *Department of Chemistry, Shaoxing University, Shaoxing, 312000, China. E-mail address: fjliu1982@gmail.com, qichenze@usx.edu.cn*

[b] *College of Chemistry and Materials Science, Hubei Engineering University, Xiaogan 432000, China.*

[c] *Wuhan Center for Magnetic Resonance, State Key Laboratory of Magnetic Resonance and Atomic and Molecular Physics, Wuhan Institute of Physics and Mathematics, Chinese Academy of Sciences, Wuhan 430071, China. Email address: zhenganm@wipm.ac.cn*

Abstract

N rich porous carbon based solid acids (NPC-[C_xN][X]) have been successfully synthesized from treating N rich porous carbon (NPC) with various quaternary ammonization reagents such as iodomethane, 1,3-propane sultone, and 1,4-butanesultone, and ion exchanging with various strong acids such as HSO_3CF_3, H_2SO_4, $H_3PW_{12}O_{40}$ and HBF_4 *etc*. The NPC support was synthesized from carbonization of polypyrrole activated with KOH without using additional templates. Various characterizations showed that NPC-[C_xN][X] possess abundant nanopores, large Brunauer-Emmett-Teller surface areas, good stability, strong and controllable acid sites with Brønsted characteristics. The immobilized acidic groups were homogeneously dispersed into NPC-[C_xN][X]. Notably, NPC-[C_xN][X] acted as efficient, reusable and generalized solid acids, which showed excellent activity in various acid-catalyzed reactions such as esterification and transesterification to the synthesis of biodiesel, dehydration of fructose into 5-hydroxymethylfurfural, depolymerization of crystalline cellulose into sugars, and condensation of phenol with acetone to the synthesis of bisphenol-A, much higher than various solid acids such as Amberlyst 15, H-ZSM-5, H-USY, and sulfonic groups functionalized ordered mesoporous silicas. The preparation of NPC-[C_xN][X] develops porous carbon based solid acids with controllable structural characteristics and excellent catalytic activity.

Key words: N rich porous carbon; Solid acids; Biomass transformation; Reusability; Controllable acid sites.

1. Introduction

Recently, carbonaceous materials with unique nanostructures have received considerable attention because of their wide applications in the areas of adsorption, separation, electrochemistry, energy storage/conversion and heterogeneous catalysis [1-13]. In the area of heterogeneous catalysis, carbonaceous materials could be used as efficient and stable catalysts and catalyst supports [1-13]. Up to now, much more research efforts have been focused on investigating the catalytic applications of carbon-metal nanocomposites or metal-free carbonaceous catalysts in various reactions such as oxidation, hydrogenation and electrocatalysis [12-20]. On the other hand, functionalization of carbonaceous materials with acidic groups to give carbonaceous solid acids have also been paid much attention because of wide applications of the solid acids in the area of green and sustainable chemistry, which are the property candidates for the replacement of mineral acids to catalyze production of various useful chemicals in industry [21-27].

Generally, the solid acids showed versatile compositions such as polymeric, inorganic and carbonaceous frameworks, carbonaceous material was suitable supports for grafting with various acidic groups because of their unique thermal, mechanical and chemical stabilities, and controllable surface wettability, which offers great opportunity for synthesizing highly efficient and reusable solid acids in industry [21]. Recently, Hara and coworkers successfully synthesized novel carbonaceous solid acids from sulfonation of the carbons derived from biomass such as glucose, sucrose

and cellulose, which developed cost effective way to the synthesis of carbonaceous solid acids [28, 29]. Nearly the same time, they successively synthesized carbonaceous solid acids with improved concentrations of acid sites from sulfonation of naphthalene at high temperature (250 °C) [30]. The resultant carbonaceous solid acids showed very good catalytic activity in esterification and condensation. However, the reported carbonaceous solid acids usually showed poor porosity, which results in the low exposure degree of catalytically active sites, further resulting in their constrained catalytic performances [21].

Introduction of abundant nanopores to give porous carbon based solid acids largely enhance the mass transfer and increase exposure degree of nonporous carbon based solid acids, which largely increases their catalytic performances in various reactions such as esterifications, condensation, transesterification, isomerization and acylation *etc* [22-26, 31, 32]. Nevertheless, the synthesis of porous carbon based solid acids usually employs various kinds of templates, and the reported template-directed synthesis was usually complicated, time consuming and high cost, which largely constrains their widely practical applications in industry [23, 24]. In the meantime, the structures of acidic sites in reported carbonaceous solid acids were basically *C*–COOH and *C*–SO_3H [25, 26, 28-30], and their constrained acid strength was not favorable for the enhancement of their catalytic activities in various acid-catalyzed reactions such as biomass transformation, esterifications and condensation.

Up to now, it is still challengeable to synthesize porous carbon based solid strong acids with controllable structures and acid sites, which will be very important for

improving their catalytic performances. Herein, we report here a template free method to synthesize novel porous carbon based solid acids (NPC-[C_xN][X]) with controllable and strong acid sites, which were synthesized from treating N rich porous carbon (NPC) with various quaternary ammonization reagents such as iodomethane, 1,3-propane sultone, and 1,4-butanesultone, and ion exchanging with strong acids such as HSO_3CF_3, H_2SO_4, $H_3PW_{12}O_{40}$, and HBF_4. The NPC support was synthesized from carbonization of polypyrrole activated with KOH without using additional templates. The resultant carbonaceous solid acids of NPC-[C_xN][X] have large Brunauer-Emmett-Teller (BET) surface areas, good thermal stability, controllable and strong acidity, and good dispersion of acid sites. The above characteristics result in NPC-[C_xN][X] with excellent activity and good reusability for catalyzing production of biofuels and fine chemicals toward transesterification and esterification to synthesis of biodiesel, depolymerization of crystalline cellulose into sugars, dehydration of fructose into 5-hydroxymethylfurfural (HMF), and condensation to the synthesis of bisphenol A, which were much better than those of reported solid acids such as Amberlyst 15, sulfonic group functionalized ordered mesoporous silicas, H-zeolites and $H_3O_{40}PW_{12}$. The preparation of NPC-[C_xN][X] will open a facile and cost effective way to the synthesis efficient and highly porous carbon based solid acids with controllable and strong acid sites, and good catalytic activity, which will be very important for their wide applications for catalyzing production of various useful chemicals and biofuels in industry.

2. Experimental section

2.1 Chemicals and reagents

All reagents were of analytical grade and used as purchased without further purification. Iodomethane, 1,3-propane sultone, and 1,4-butanesultone, HSO_3CF_3, H_2SO_4, CH_2Cl_2, toluene, glucose, tetraethyl orthosilicate (TEOS), NaOH, pyrrole, $FeCl_3 \cdot 6H_2O$, potassium sodium tartrate, sodium sulfite, methanol, 3,5-dinitrosalicylic acid, $H_3PW_{12}O_{40}$, phenol, KOH and acetone were obtained from Sinopharm Chemical Reagent, Beijing Co., Ltd. Crystalline cellulose of Avicel (extra pure, average particle size 50 μm, crystalline degree: 80~90 %), 3-mercaptopropyltrimethoxysilane (3-MPTS), nonionic block copolymer surfactant poly(ethyleneoxide)-poly(propyleneoxide)-poly(ethyleneoxide) block copolymer (P123), Amberlyst 15, tripalmitin, 1-n-butyl-3-methylimidazolium chloride ($[C_4mim]Cl$ ionic liquid), palmitic acid, fructose, 1-vinylimidazole, tripalmitin and HMF were purchased from Sigma-Aldrich Co.

2.2 Synthesis of NPC

NPC was synthesized from carbonization of polypyrrole (PPy) in presence of KOH activated reagent, and PPy precursor was synthesized from polymerization of pyrrole initiated with $FeCl_3$ in aqueous media. Typically, 3 g of pyrrole (purified) was slowly added into a solution containing 0.5 mol of $FeCl_3$ and 200 mL of water, after magnetically stirring of the mixture for 3 h at room temperature, abundant black

precipitate was formed at the bottom of glassware. The PPy could be obtained from filtration, washing with abundant water to remove all the $FeCl_3$ initiator, and drying at 80 °C under vacuum conditions. The final yield of polypyrrole was nearly to 100 %. To get N rich porous carbon, the resultant PPy and KOH with different weight ratios (0.25~1) was mixed together, and carbonization at 600-850 °C. Typically, 1.0 g of PPy was well mixed with 2.0 g of anhydrous KOH, then the mixture was carbonized at 800 °C for 1 h under flowing N_2 conditions with the heating rate of 3 °C·min^{-1}. Finally, the chemically activated samples were thoroughly washed several times with HCl (10 *wt*%) to remove any inorganic salts, washing with abundant water until neutral, and drying at 120 °C under vacuum conditions, NPC samples with abundant nanopores were obtained.

2.3 Synthesis of carbonaceous solid acids of NPC-[C_3N][X]

NPC-[C_3N][X] were synthesized from quaternary ammonization of NPC by using 1,3-propanesultone, and anion exchanging with strong acids of HSO_3CF_3, H_2SO_4, $H_3PW_{12}O_{40}$, or HBF_4. (In the sample of NPC-[C_3N][X], [X] stands for the treating acid ions and C_3 stands for quaternary ammonization reagent of 1,3-propanesultone, which contains three carbon atoms). In addition, NPC-[C_1N][X] and NPC-[C_4N][X] could also be successfully prepared by using iodomethane and 1,4-butanesultone as quaternary ammonization reagents respectively. As a typical run for synthesizing NPC-[C_3N][SO_3CF_3], 1.0 g of NPC was dispersed into a mixture contains 20 mL of toluene and 0.5 g of 1,3-propanesultone, after stirring of the reaction mixture at

110 °C for 24 h under refluxing, the reaction was finished and the mixture was cooled down to room temperature (25 °C). The resultant sample of NPC-$[C_3N]^+$ could be obtained from centrifugation, washing with abundant CH_2Cl_2 and drying at 60 °C under vacuum conditions. To get NPC-$[C_3N][SO_3CF_3]$, NPC-$[C_3N]^+$ was then dispersed into a solution containing 25 mL of toluene and 3-5 mL HSO_3CF_3, after stirring of the mixture for 48 h at 0 °C, NPC-$[C_3N][SO_3CF_3]$ could be obtained from centrifugation, washing with abundant CH_2Cl_2 to remove the residual HSO_3CF_3, and drying at 60 °C for 12 h under vacuum conditions. The ion exchanging procedure was repeated twice. Except for HSO_3CF_3, other strong acids such as H_2SO_4, $H_3PW_{12}O_{40}$ and HBF_4 could also be used as acid-exchanged reagents, which results in the samples with controllable acid sites. For comparison, SBA-15-SO_3H (S/Si=0.2, "SBA" stands for ordered mesoporous silicas) was synthesized according to the literature [33].

2.4 Characterization methods

Nitrogen isotherms were measured by using a Micromeritics ASAP 2020M system. The samples were outgassed for 10 h at 150 °C before the measurements were taken. The mesopore-size distribution was calculated using the Barrett-Joyner-Halenda (BJH) model and micropore-size distribution was calculated using the Horvath-Kawazoe (HK) model. FT-IR spectra were collected by using a Bruker 66V FT-IR spectrometer. Raman spectra were measured by using a LabRam Aramis Raman Microscope system (Horiba-Jobin Yvon). X-ray powder diffraction (XRD) of samples was recorded on a Rigaku D/max2550 PC powder diffractometer,

using nickel-filtered CuKα radiation at approximately 10°≤2θ≤80°. Transmission electron microscopy (TEM) images were taken on a JEM-2100 electron microscope (JEOL, Japan) with an acceleration voltage of 200 kV. CHNS elemental analysis was performed on a Perkin-Elmer series II CHNS analyzer 2400. XPS spectra were performed on a Thermo ESCALAB 250 with Al Kα radition at *y*=901 for the X-ray sources. The binding energies were calibrated using the C1s peak at 284.9 eV. Differential thermal analysis (DTA) and thermogravimetric analysis (TG) were tested by a Perkin-Elmer TGA7 under both flowing air and N_2 conditions with the heating rate of 10 °C/min. Scanning electron microscopy (SEM) images, energy-dispersive X-ray spectroscopy (EDX) spectra, and elemental maps were performed on an FEI Strata 400S DualBeam system with an acceleration voltage of 15 kV.

The solid ^{31}P NMR spectrum over NPC-[C_3N][SO_3CF_3] was performed as follows: prior to the adsorption of probe molecules, the solid acids were placed in glass tubes and then connected to a vacuum line for dehydration. The temperature was gradually increased at a rate of 1 °C/min, and the samples were kept at a final temperature of 393 K at a pressure below 10^{-3} Pa, over a period of 12 h. After the samples cooled to ambient temperature, a sufficient amount of trimethylphosphine (TMP) was introduced into the acidic samples, with the activated samples frozen by liquid N_2, followed by elimination of the physisorbed probe molecules by evacuation at room temperature for 30 minutes. Finally, the sample tubes were flame sealed. The preparation of trimethylphosphine oxide (TMPO) adsorbed samples was performed according to the method proposed by our previous work [34]. Prior to the NMR

experiments, the sealed sample tubes were opened and the samples were transferred into ZrO_2 rotors with a Kel-F end cap under a dry nitrogen atmosphere in a glovebox.

All the NMR experiments were performed on a Bruker Ascend-500 spectrometer at resonance frequencies of 500.57, 202.63 and 125.88 MHz for ^{1}H, ^{31}P and ^{13}C, respectively, with a 4 mm triple-resonance MAS probe at a spinning rate of 10 kHz. A $\pi/2$ pulse width of 4.7 μs and a recycle delay of 15 s were used for ^{13}C NMR experiment. ^{31}P MAS NMR spectra with high power proton decoupling were recorded using a $\pi/2$ pulse length of 3.2 us and a recycle delay of 30 s. The chemical shift of ^{13}C was externally referenced to adamantane, while that of ^{31}P was referenced to 1 M aqueous H_3PO_4.

2.5 Catalytic reactions

2.5.1 Transesterification

Transesterification of tripalmitin with methanol was executed as follows: 1.68 g (2.08 mmol) of tripalmitin was melted into a flask equipped with a condenser and magnetic stirrer at 65 °C, followed by addition of 0.20 g of catalyst upon vigorous stirring to form a homogeneous mixture. Then, an additional 7.41 mL (187.2 mmol) of methanol acts as both reactant and solvent was rapidly added, after further stirring of the mixture for 14 h at 65 °C under refluxing, the reaction was finished. The catalysts could be separated from reaction mixture from centrifugation. The molar ratio of tripalmitin/methanol was 1/90 and the mass ratio of catalyst/tripalmitin was 0.119.

2.5.2 Esterification

Esterification of fatty acid of palmitic acid with methanol was executed as follows: 1.282 g of palmitic acid (5 mmol) and 2.5 mL of methanol were added into a flask equipped with a condenser and magnetic stirrer, then 0.05 g of catalyst was quickly introduced into the mixture under vigorous stirring. The reaction was performed at 65 °C for 5 h. At different time intervals, samples were withdrawn and analyzed by using gas chromatography.

The product in both trasesterification and esterification was methyl palmitate with selectivity near 100 %, which was analyzed by using gas chromatography of Agilent 7890A equipped with a flame ionization detector (FID). The column was HP-INNOWax capillary column (30 m); the initial temperature was 100 °C, ramping rate was 20 °C/min, and the final temperature was 280 °C; the temperature of FID detector was 300 °C. In this reaction, the concentration of methyl palmitate was calculated through the internal standard (dodecane) method, and established the corresponding correction factor.

2.5.3 Catalysts regeneration

In the reaction of transesterification of tripalmitin with methanol: 1.68 g (2.08 mmol) of tripalmitin and 0.20 g of catalyst were mixed into a flask equipped with a condenser and magnetic stirrer at 65 °C, followed by addition of 7.41 mL (187.2 mmol) of methanol, which acts as both reactant and solvent was rapidly added. After stirring of the mixture for 14 h at 65 °C under refluxing, the catalysts could be

separated by centrifugation, washing with abundant CH_2Cl_2 to remove the absorbed reactants and products and drying it at 60 °C under vacuum condition, which was used directly for the next run.

2.5.4 Catalyze depolymerization of crystalline cellulose

Depolymerization of crystalline cellulose (Avicel) was also chosen as the model reaction for evaluating the activities of various solid acids. Typically, 100 mg of crystalline cellulose of Avicel was dissolved into 2.0 g of $[C_4mim]Cl$ ionic liquid at 100 °C for 3-5 h under vigorous stirring until a clear solution was obtained, followed by addition of 20 mg of NPC-$[C_3N][SO_3CF_3]$. Then, 600 μL of water (reactant) was slowly introduced into the reaction mixture, and the reaction temperature was kept at 100 °C. At different time intervals, samples were withdrawn, weighed, quenched immediately with cold water, and centrifuged at 13,500 rpm for 5 min to remove catalysts and unreacted cellulose, which gives the reaction mixture. For comparison, various acid catalysts such as Amberlyst 15, H-ZSM-5, H-USY and SBA-15-SO_3H were also used for catalyzing depolymerization of Avicel under the same condition.

Meanwhile, the isolated cellulose was thoroughly washed with water, and recovered through centrifugation. The amount of cellulose isolated could be determined by weight.

2.5.5 Testing Total Reducing Sugars (TRS)

TRS value was used for evaluating the depolymerization degree of crystalline

cellulose catalyzed by various catalysts, which was tested through DNS method [22]. Typically, a mixture containing of 0.1 mL of 3,5-dinitrosalicylicacid (DNS) reagent and 0.1 mL of performed reaction mixture was heated for 5 min at 100 °C, then cooled to room temperature, followed by addition of 0.8 mL of deionized water to dilute the mixture. The color intensity of the mixture was measured in a NanoDrop 2000 UV-spectrophotometer at the wavelength of 540 nm. The concentration of the total reducing sugars was calculated based on the standard curve method.

2.5.6 Catalyze transformation of fructose

Catalyze transformation of fructose into HMF and furan-2,5-dicarbaldehyde was performed with the following procedures: 0.1 g of fructose and 20 mg of catalyst were added into a mixture containing 3 g of THF and 2 g of DMSO, which was heated at 100 °C for 10 h. The major products were HMF and furan-2,5-dicarbaldehyde, and the major by-products were LA, FA and some others.

2.5.7 Catalyze synthesis of bisphenol-A

Catalyze synthesis of bisphenol-A was performed through condensation of phenol with acetone in presence of various solid acids. Typically, 70 mmol phenol and 10 mmol acetone were mixed together, followed by addition of 0.07 g of solid acid catalysts, the reaction mixture was heated at 85 °C for 24 h in a flask equipped with a

condenser and magnetic stirrer. The main products were *p,p′*-bisphenol-A and *o,p*-bisphenol-A.

2.5.8 Analysis of products

In the reaction of depolymerization of crystalline cellulose, the concentrations of the sugars were measured by Shimadzu LC-20A high-performance liquid chromatography (HPLC) system equipped with a refractive index detector based on standard curve method, which was separated with a SCR-101N column using extra-pure water during mobile phase at a flow rate of 0.5 mL/min. The column's temperature was set to 50 °C. On the other hand, the yields of *p,p′*-bisphenol-A and *o,p*-bisphenol-A, HMF, furan-2,5-dicarbaldehyde and other byproducts were also measured by Shimadzu LC-20A HPLC system based on standard curve method. It was equipped with a CAPCELL PAK C_{18} column using methanol and water (methanol/water=80:20) as the mobile phase, with a flow rate of 0.7 mL/min and the column's temperature was set to 50 °C. In the meantime, an ultraviolet detector with the wavelength number at 249 and 254 nm was used to detect these products.

3. Results and discussion

Figure 1 showed XRD patterns of NPC, NPC-$[C_3N][SO_3CF_3]$. For the sample of NPC, two broad peaks at around 2θ=24.9 and 43.3 ° could be observed, which

indicates its amorphous characteristics [35]. After functionalization of NPC with strongly acidic groups, giving the sample of NPC-[C_3N][SO_3CF_3], which exhibited similar peaks at around 2θ=24.9 and 43.3 ° with decreased diffraction intensity in comparison with that of NPC. Consideration of the amorphous network of both NPC and NPC-[C_3N][SO_3CF_3], the decreased intensity in NPC-[C_3N][SO_3CF_3] may be attributed to the grafting of strong acidic groups, which results in formation of various defects sites on the network of NPC-[C_3N][SO_3CF_3]. In addition, several peaks associated with $H_3PW_{12}O_{40}$ could also observed in NPC-[C_3N][$H_2PW_{12}O_{40}$], which indicates heteropolyacid of $H_3PW_{12}O_{40}$ could also be immobilized into NPC support (Figure S1). The above results confirm controllable and strong acid sites were formed in NPC-[C_xN][X].

Figure 2 showed Raman spectra of NPC and NPC-[C_3N][SO_3CF_3], both of them showed two broad peaks associated with D-band and G-band, respectively. Notably, the D-band was attributed to sp3 carbon atoms in the network in these samples; while G-band was attributed to sp2 carbon atoms in a graphitic 2D hexagonal lattice in these samples. Compared with G-band peaks, the obviously stronger D-band peaks in NPC and NPC-[C_3N][SO_3CF_3] indicated their typically amorphous carbon network. In addition, broad peaks ranging from 2400 to 3000 cm^{-1} associated with the signal of 2D band could also observed in the second-order Raman spectra in both samples, which further confirms amorphous network, the presence of high proportions of edge planes and structure defects in these samples [36]. Compared with NPC, the decreased G-band of NPC-[C_3N][SO_3CF_3] may be attributed to formation of various defects

sites on its network, which should be resulted from grafting of acidic groups, in good agreement with XRD results.

Figure 3 showed N_2 isotherms and pore size distribution of NPC, NPC-$[C_3N]^+$ and NPC-$[C_3N][SO_3CF_3]$. Notably, a steep increase in the curve at a relative pressure of $10^{-6}<P/P_0<0.01$ due to the filling of micropores could be clearly observed in these samples, which confirm abundant micropores (~0.64 nm) was formed in the samples [37]. After acidification of NPC to give the sample of NPC-$[C_3N]^+$ and NPC-$[C_3N][SO_3CF_3]$. NPC-$[C_3N]^+$ gave an additional small hysteresis loop at a relative pressure $0.5<p/p_0<0.8$ (Figure 3b) in comparison with NPC support, which gave the pore size at around 4 nm. Further treating of NPC-$[C_3N]^+$ with strong acid of HSO_3CF_3, giving the sample of NPC-$[C_3N][SO_3CF_3]$, which showed typical-IV isotherms with an enhanced hysteresis loop at a relative pressure $0.5<p/p_0<0.8$ (Figure 3c). The pore size distribution of resultant NPC-$[C_3N][SO_3CF_3]$ was also centered at around 4 nm. The above results indicated that acidification of NPC may result in the broken of bulky NPC monolith into nanoscaled particles, and the metastable nanoparticles quickly aggregated again, which results in the formation of additional mesopores in NPC-$[C_3N]^+$ and NPC-$[C_3N][SO_3CF_3]$ [33]. Compared with NPC support, the decreased BET surface area (1600 Vs 525 m^2/g) and pore volume (0.82 Vs 0.36 cm^3/g) of NPC-$[C_3N][SO_3CF_3]$ should be attributed to the grafting of acidic groups in the sample, which largely increases the weight and blocks the nanopores of the sample (Table 1), similar results have also been reported previously [32]. Notably, the BET surface area of NPC-$[C_3N][SO_3CF_3]$ was higher than those of Amberlyst 15, and

ZSM-5, lower than those of USY zeolite and sulfonic group functionalized mesoporous silica (SBA-15-SO_3H) (Table 1). The abundant nanoporous structures could also be observed in the sample of NPC-[C_3N][$H_2PW_{12}O_{40}$] (Figure S2).

Figure 4 showed SEM images of NPC-[C_3N][SO_3CF_3], which exhibited monolithic morphology with disordered shapes. In the meantime, the enlarged images of NPC-[C_3N][SO_3CF_3] gave the rough surface characteristics, which may be attributed to presence of nanopores in the sample. Moreover, the EDX spectrum and elemental maps of NPC-[C_3N][SO_3CF_3] have also been carefully investigated, which were efficient tools for characterization of the elemental components and dispersion state. Interestingly, NPC-[C_3N][SO_3CF_3] showed the signals of C, N, O, and S elements, which were homogeneously dispersed into NPC-[C_3N][SO_3CF_3] (As shown in Figure 5 C-F). Notably, the content of S obtained from EDX result (6.21 %) was similar with the result obtained from elemental analysis (6.7 %, Table 1), which was higher than that of SBA-15-SO_3H, lower than that of Amberlyst 15. The above results confirm that acidic groups have been successfully grafted onto the network of NPC.

Figure 6 showed TEM images of NPC-[C_3N][SO_3CF_3], which exhibited monolithic morphology with abundant nanopores. In addition, the high-resolved TEM images showed that NPC-[C_3N][SO_3CF_3] has abundant worm-hole like micropores, which exhibited amorphous characteristics, in agreement with XRD, Raman and N_2 isotherms results. Except for micropores, NPC-[C_3N][SO_3CF_3] also showed abundant mesopores (Figure 6A), which was formed through aggregating of small particles, in agreement with N_2 isotherms results. In general, the acidification of NPC may result

in the broken of bulky monolith into nanoscaled particles, and the metastable nanoparticles aggregated again to form additional mesopores in NPC-$[C_3N][SO_3CF_3]$ in comparison with NPC support. The above results confirm the template free route exploited by us could be used for preparation of porous carbon based solid acid, and the abundant nanopores of NPC-$[C_3N][SO_3CF_3]$ largely enhance the fast diffusion of reactants and products in various acid-catalyzed reactions.

Figure 7 showed TG and DTA curves of NPC and NPC-$[C_3N][SO_3CF_3]$, which was an efficient way for investigation of thermal stability of various materials. Notably, NPC showed the weight loss at the temperature stages ranging from 30-100 and 480-590 °C, which should be attributed to losing of absorbed water and the destruction of its carbonaceous network, the higher decomposition temperature of NPC indicates its very good thermal stability for usage as catalyst support. After grafting acidic groups onto NPC, giving the sample of NPC-$[C_3N][SO_3CF_3]$, which exhibited the weight loss associated with the desorption of water, decomposition of acidic group, and destruction of carbonaceous network at the temperature stages ranging from 30-100, 190-330, and 450-550 °C, respectively (Figure 7A). Similar results could also be observed in DTA curves (Figure 7B). The high decomposition temperatures of both acidic group and carbonaceous network in NPC-$[C_3N][SO_3CF_3]$ indicates its very good thermal stability, which was very important for it used as stable and reusable solid acid in various acid-catalyzed liquid reactions. Compared with NPC, the decreased temperature of the destruction of carbonaceous network should be attributed to presence of oxygen containing groups such as –OH in the

sample, which was resulted from the treatment of carbonaceous network with 1,3-propanesultone and ultra strong acids of HSO_3CF_3.

Figure 8 showed the X-ray photoelectron spectroscopy (XPS) spectra of NPC-$[C_3N][SO_3CF_3]$, which exhibits the signals of S_{2p} (168.6 eV), C_{1s} (285.4 eV), N_{1s} (400.8 eV), O_{1s} (532.7 eV) and F_{1s} (688.4 eV) because of grafting of -$[C_3N][SO_3CF_3]$ group onto NPC support. Notably, the broad signal of C_{1s} could be fitted and deconvoluted into four peaks (284.8, 286.3, 287.8 and 292.3 eV), which should be assigned to C-C and C-N bond in NPC network, and C-S and C-F bond in -$[C_3N][SO_3CF_3]$ group, respectively [32, 38]. In addition, two broad peaks associated with N_{1s} were centered at approximately 399.1 and 401.2 eV, which should be attributed to the signals of C-N and $[C_3N]$ group in NPC-$[C_3N][SO_3CF_3]$ [31, 36]. Similarly, the signals of O_{1s} associated with $–SO_3H$ (531.5 eV) and O-SCF_3 (532.8 eV) could also be clearly observed [32, 38]. The above results indicate that strong acidic group has been successfully grafted onto the network of NPC, in good agreement with elemental analysis and elemental maps results (Table 1). Correspondingly, FT-IR spectrum further confirms the above results (As shown in Figure 9), the peaks at around 683, 1068 and 1179 cm^{-1} should be assigned to the signals of C-S and S=O bond in the sample, and the peak at around 1282 cm^{-1} should be assigned to the signal of C-F bond, which further confirm the successfully grafting of strong acidic group onto NPC support.

Figure 10 showed ^{13}C solid NMR spectrum of NPC-$[C_3N][SO_3CF_3]$. The strong peak at around 16 ppm should be assigned to $\underline{C}H_3$ carbon in C_3N group or NPC

network. The peaks at around 61 and 49 ppm are assigned to methylene carbon linked with sulfonic group and nitrogen in C_3N group [39], which is indicative that the [$-CH_2CH_2CH_2SO_3H$] group has been bonded onto NPC network. Notably, the peak at around 68 ppm should be assigned to *C*-OH carbon, which maybe resulted from partial oxidation of NPC network during acidification processes. Alternatively, the broad peaks at around 129 and 139 ppm should be assigned to the C-C and C-N bond in NPC network. The above results indicated strong acidic group has been successfully grafted onto the network of NPC, in good agreement with XPS and FT-IR spectra results.

Figure 11 showed the ^{31}P NMR probe spectra of NPC-[C_3N][SO_3CF_3], which involves the adsorbed trimethylphosphine (TMP) and trimethylphosphine oxygen (TMPO). It is well known that the ^{31}P NMR probe technique is a sensitive and reliable technique to characterize the acidity (Acid types and strength) of various solid acids [34, 40, 41]. In Figure 11a, TMP was used as a probe molecule, and the peak at around -3.4 ppm was assigned to the protonated adducts of $[(CH_3)_3P\text{-}H]^+$, which was resulted from the reaction between TMP and typically Brønsted acidic protons. On the contrary, the peaks ranged from -20 to -60 ppm associated with the interaction between TMP and Lewis acid sites could not be found [34, 40], which indicates that typically Brønsted acid sites was formed in NPC-[C_3N][SO_3CF_3]. In the meantime, solid-state ^{31}P MAS NMR spectrum of adsorbed TMPO by NPC-[C_3N][SO_3CF_3] was also carefully investigated, which could accurately determine the acid strength of various solid acids such as zeolites, sulfonic group functionalized mesoporous silica, sulfated

mesoporous metal oxides and heteropolyacids [39, 40]. Interestingly, NPC-[C_3N][SO_3CF_3] showed multiple ^{31}P resonance peaks at around 45, 53, 64, and 80 ppm, which indicates the acid sites with different acid strength were formed in NPC-[C_3N][SO_3CF_3] (Figure 11b). The weak acidic sites (45 ppm) may be attributed to hydroxyl groups in NPC-[C_3N][SO_3CF_3]; While the relative strongly acidic site at around 53 ppm may be attributed to protonated nitrogen atom in NPC network by HSO_3CF_3, which may form the structure of NPC-[N^+H][SO_3CF_3]. Interestingly, the strong acidic sites at around 64 and 80 ppm should be attributed to sulfonic group and acidic ionic liquids group located over NPC-[C_3N][SO_3CF_3] catalyst surfaces. The aforementioned results directly confirmed strong and controllable acidic group has been grafted onto NPC support, which result in the formation of NPC-[C_3N][SO_3CF_3]. NPC-[C_3N][SO_3CF_3] showed relatively strong acidity in comparison with those of HY zeolites (55 and 65 ppm) and bifunctional carbon-silica nano composited solid acid (40-70 ppm) based on the ^{31}P chemical shift of adsorbed TMPO probe [41, 42]. Therefore, this novel catalyst possibly has a better catalytic role for the acid catalyzed reactions for its unique structure and controllable acidity.

Figure 12 showed catalytic kinetics curves in transesterification of tripalmitin with methanol catalyzed by various samples, which was thought to be an efficient way for production of biodiesel [32]. Notably, NPC-[C_3N][SO_3CF_3] showed much improved catalytic activity in comparison with conventional solid acids such as SBA-15-SO_3H, Amberlyst 15 and H-form ZSM-5 zeolite, which was as comparable as that of homogeneous heteropolyacid of $H_3PW_{12}O_{40}$. For instance, after 6 h of

incubation, the yield of methyl palmitate catalyzed by NPC-[C_3N][SO_3CF_3] was 52.5 %. On the contrary, the yields of methyl palmitate catalyzed by $H_3PW_{12}O_{40}$, SBA-15-SO_3H, and Amberlyst 15 were 32.4, 26.0 and 21 %, respectively; Further prolonging the reaction time up to 14 h, the yield of methyl palmitate catalyzed by NPC-[C_3N][SO_3CF_3] was increased up to 82.9 %, much higher that those of $H_3PW_{12}O_{40}$ (70.1 %), SBA-15-SO_3H (57.2 %), and Amberlyst 15 (49.6 %). Nevertheless, the yield of methyl palmitate catalyzed by H-form ZSM-5 (10.8 %) was very low even the reaction time was increased up to 14 h because of its constrained micropores, which strongly restrict its catalytic applications for bulky molecules. Moreover, NPC-[C_3N][SO_3CF_3] also showed good reusability. For instance, even after being recycled for 5 times, very little decreased yield of methyl palmitate catalyzed by recycled NPC-[C_3N][SO_3CF_3] should be resulted from the coverage of acidic sites by reactants and products (Figure 12b). The above results confirmed that NPC-[C_3N][SO_3CF_3] act as highly efficient and stable solid acids for catalyzing biodiesel production.

Furthermore, the catalyze production of biodiesel through esterification of fatty acid with methanol has also been carefully investigated in this work. Figure 13 showed the catalytic kinetics curves of palmitic acid with methanol catalyzed by various solid acids. Notably, NPC-[C_3N][SO_3CF_3] showed much improved activity in comparison with various solid acids. For instance, only for 1 h, the yield of methyl palmitate catalyzed by NPC-[C_3N][SO_3CF_3] was up to 90.8 %, much higher than those Amberlyst 15 (55.2 %), SBA-15-SO_3H (55.2 %), and H-ZSM-5 (3.5 %), which

was as comparable as that of $H_3PO_{40}W_{12}$ (90.2 %). Further prolonging the reaction time to 3 h, the yield of methyl palmitate catalyzed by NPC-$[C_3N][SO_3CF_3]$ was nearly 100 %, while Amberlyst 15, SBA-15-SO_3H, H-ZSM-5, and $H_3PO_{40}W_{12}$ gave relatively low yields at 73.5, 76.8, 11.6, and 96.9 %, respectively.

On the other hand, NPC-$[C_3N][SO_3CF_3]$ type of solid acids were also very active in other biomass transformation reactions such as fructose dehydration into HMF and depolymerization of crystalline cellulose into sugars. Table 2 presents the activities of various acidic catalysts for catalyzing fructose dehydration, which was an important model reaction for transformation sugars into useful chemicals [22, 43-45]. Notably, NPC-$[C_3N][SO_3CF_3]$ showed excellent catalytic activity and products selectivity in comparison with those of Amberlyst 15, SBA-15-SO_3H, and H-ZSM-5. For instance, the yields of two main products of HMF and furan-2,5-dicarbaldehyde catalyzed by NPC-$[C_3N][SO_3CF_3]$ were 79.5 and 8.1 % after 10 h of reaction, much higher than those of SBA-15-SO_3H (53.2 & 4.1 %), H-ZSM-5 (38.6 & 3.7 %), and Amberlyst 15 (50.3 & 4.6 %). Similar superior activity could also be observed in NPC-$[C_3N][SO_4H]$ (80.1 & 7.8 %). More importantly, NPC-$[C_3N][SO_3CF_3]$ showed very good reusability, even after being recycled for five times, the yields of HMF and furan-2,5-dicarbaldehyde catalyzed by recycled NPC-$[C_3N][SO_3CF_3]$ (77.2 & 7.5 %) were even as comparable as those of fresh NPC-$[C_3N][SO_3CF_3]$ (79.5 & 8.1 %, Table 2, Run 1).

In the meantime, NPC-$[C_3N][SO_3CF_3]$ also showed very good activity for catalyzing depolymerization of crystalline cellulose into sugars: an important reaction

in the areas of biomass transformation, which showed potentially important applications in industry because of very large storage and low cost of crystalline cellulose in nature [22]. For instance, after 5 h of incubation, the yields of TRS catalyzed by NPC-[C_3N][SO_3CF_3] and NPC-[C_3N][SO_4H] were up to 78.5 and 79.2 % respectively, much higher than those of conventional solid acids including Amberlyst 15 (60.2 %), SBA-15-SO_3H (51.8 %), H-ZSM-5 (26.7 %), and H-USY (42.6 %). Correspondingly, the yields of main products of glucose, cellobiose and HMF catalyzed by NPC-[C_3N][SO_3CF_3] (50.3, 17.3 and 9.8 %) and NPC-[C_3N][SO_4H] (47.5, 22.3 and 9.2 %) were much higher than those of Amberlyst 15 (30.3, 18.4 and 4.6 %), SBA-15-SO_3H (25.4, 13.6 and 4.1 %), H-ZSM-5 (10.4, 7.6 and 2.8 %), and H-USY (22.5, 11.2 and 3.5 %, Table 3). The catalytic data also indicated relatively good selectivity for glucose and HMF catalyzed by NPC-[C_3N][SO_3CF_3] and NPC-[C_3N][SO_4H] (Table 3). The above results confirmed that NPC-[C_3N][SO_3CF_3] and NPC-[C_3N][SO_4H] act as novel and efficient solid acids for catalyzing biomass transformations.

At last, we successively expand the catalytic applications of NPC-[C_3N][SO_3CF_3] in condensation of phenol with acetone, which was an important reaction for synthesis of bisphenol-A. More importantly, NPC-[C_3N][SO_3CF_3] showed much improved activity in comparison with above solid acids (Table 4). For instance, after 24 h of incubation, the conversions of phenol catalyzed by NPC-[C_3N][SO_3CF_3] and NPC-[C_3N][SO_4H] were 21.4 and 22.5 % respectively, which gave the TOF values at 3.8 and 3.75 h^{-1} respectively (The completed conversion of phenol through

theoretical calculation is 28.6%), similar results could also be observed in NPC-[C_3N][$H_2PW_{12}O_{40}$] (20.6, 4.1 h^{-1}). On the contrary, Amberlyst 15, SBA-15-SO_3H, H-USY and H-ZSM-5 gave relatively low conversions of phenol at 13.4, 10.9, 8.7 and 4.8 %, which exhibited the TOF values at 1.2, 3.3, 2.0 and 5.0, respectively. It is noteworthy that all the solid acids showed similar selectivity for the products of *p,p'*-bisphenol-A and *o,p*-bisphenol-A.

The above results confirm that NPC-[C_3N][SO_3CF_3] could be used as highly efficient and reusable carbon based solid acids in various acid-catalyzed reactions. The excellent activity and reusability found in NPC-[C_3N][SO_3CF_3] should be attributed to their unique characteristics including large BET surfaces, abundant nanopores, good stability, controllable and strong acidity. The large surface area and abundant nanopores strongly enhance the fast diffusion of reactants and products in the samples, further resulting in much improved exposure degree of acidic sites in NPC-[C_3N][SO_3CF_3]. Moreover, controllable and strong acidity of NPC-[C_3N][SO_3CF_3] effectively decrease the activation energy in these reactions. The above advantages make NPC-[C_3N][SO_3CF_3] acts as highly efficient and reusable solid acids in various reactions, further consideration of their facile and cost-effective synthetic processes, which will be very important for their widely practical applications in the area of heterogeneous acid catalysis.

4. Conclusions

N rich porous carbon was synthesized from carbonization of polypyrrole in

presence of KOH without using additional templates, which was used as novel and stable support for grafting with strong acidic groups, the resultant NPC-[C_xN][X] type of solid acids showed large BET surface areas, good stability, abundant nanopores, controllable and strong acidity. The above characteristics result in NPC-[C_xN][X] with much improved activity and good reusability for catalyzing biomass transformations and fine chemical synthesis. The preparation of NPC-[C_xN][X] will develop a new way to synthesize efficient and reusable carbonaceous solid acids with controllable nanopores and strong acid sites, and good catalytic activities, which will be very important for the wide applications of carbonaceous solid acids in the area of heterogeneous acid catalysis.

Acknowledgements: This work was supported by the National Natural Science Foundation of China (21573150, 21203122, 21473244, 21522310), Natural Science Foundation of Zhejiang Province (LY15B030002). Foundation of State Key Laboratory of Magnetic Resonance and Atomic, Molecular Physics, Wuhan Institute of Physics and Mathematics, Chinese Academy of Sciences (T151303).

References

1 R. Ryoo, S. H. Joo and S. Jun, *J. Phys. Chem. B* 1999, **103**, 7743.

2 F. Su, J. Zeng, X. Bao, Y. Yu, J. Y. Lee and X. S. Zhao, *Chem. Mater.* 2005, **17**, 3960.

3 Y. P. Zhai, Y. Q. Dou, D. Y. Zhao, P. F. Fulvio, R. T. Mayes and S. Dai, *Adv. Mater.* 2011, **23**, 4828.

4 K. S. Novoselov, A. K. Geim, S. V. Morozov, D. Jiang, Y. Zhang, S. V. Dubonos, I. V. Grigorieva and A. A. Firsov, *Science* 2004, **306**, 666.

5 K. S. Noveselov, A. K. Geim, S. V. Morozov, D. Jiang, M. I. Katsnelson, I. V. Grigorieva, S. V. Dubonos and A. A. Firsov, *Nature* 2005, **438**, 197.

6 D. S. Su, S. Perathoner and G. Centi, *Chem. Rev.* 2013, **113**, 5782.

7 S. Iijima, *Nature* 1991, **354**, 56.

8 Y. Meng, D. Gu, F. Q. Zhang, Y. F. Shi, H. F. Yang, Z. Li, C. Z. Yu, B. Tu and D. Y. Zhao, *Angew. Chem., Int. Ed.* 2005, **44**, 7053.

9 C. D. Liang and S. Dai, *J. Am. Chem. Soc.* 2006, **128**, 5316.

10 X.-H. Li, S. Kurasch, U. Kaiser and M. Antonietti, *Angew. Chem. Int. Ed.* 2012, **51**, 9689.

11 P. P. Su, L. Jiang, J. Zhao, J. W. Yan, C. Li and Q. H. Yang, *Chem. Commun.* 2012, **48**, 8769.

12 Y. Wang, J. Yao, H. R. Li, D. S. Su and M. Antonietti, *J. Am. Chem. Soc.* 2011, **133**, 2362.

13 P. F. Zhang, Y. T. Gong, H. R. Li, Z. R. Chen and Y. Wang, *Nat. Comm.* 2012, **4**, 1593.

14 K. Woan, G. Pyrgiotakis and W. Sigmund, *Adv. Mater.* 2009, **21**, 2233.

15 A. Thomas, A. Fischer, F. Goettmann, M. Antonietti, J.-O. Müller, R. Schlögl and J. M. Carlsson, *J. Mater. Chem.* 2008, **18**, 4893.

16 J. Zhang, X. Liu, B. Raoul, A. H. Zhang, R. Schlögl and D. S. Su, *Science* 2008, **322**, 73.

17 G.-L. Chai, Z. F. Hou, D.-J. Shu, T. Ikeda and K. Terakura, *J. Am. Chem. Soc.* 2014, **136**, 13629.

18 K. Wan, G.-F. Long, M.-Y. Liu, L. Du, Z.-X. Liang and P. Tsiakaras, *App. Catal. B: Environ.* 2015, **165**, 566.

19 C. H. Choi, H.-K. Lim, M. W. Chung, C. P. Jong, H. Shin, H. Kim and S. Woo, *J. Am. Chem. Soc.* 2014, **136**, 9070.

20 P. Serp, M. Corrias and P. Kalck, *App. Catal. A-Gen.* 2003, **253**, 337.

21 F. J. Liu, J. Sun, L. F. Zhu, X. J. Meng, C. Z. Qi and F.-S. Xiao, *J. Mater. Chem.* 2012, **22**, 5495.

22 J. S. Luterbacher, D. Martin Alonso and J. A. Dumesic, *Green Chem.* 2014, **16**, 4816.

23 X. Q. Wang, R. Liu, M. M. Waje, Z. W. Chen, Y. S. Yan, K. N. Bozhilov and P. Y. Feng, *Chem. Mater.* 2007, **19**, 2395.

24 R. Xing, Y. M. Liu, Y. Wang, L. Chen, H. H. Wu, Y. W. Jiang, M. Y. He and P. Wu, *Micro. Meso. Mater.* 2007, **105**, 41.

25 X. Z. Liang, M. F. Zeng and C. Z. Qi, *Carbon* 2010, **48**, 1844.

26 J. F. Pang, A. Q. Wang, M. Y. Zheng and T. Zhang, *Chem. Comm.* 2010, **46**, 6935.

27 X. M. Zhang, Y. P. Zhao, S. T. Xu, Y. Yang, J. Liu, Y. X. Wei and Q. H. Yang, *Nat. Comm.* 2013, **5**, 3170.

28 S. Suganuma, K. Nakajima, M. Kitano, D. Yamaguchi, H. Kato, S. Hayashi and M. Hara, *J. Am. Chem. Soc.* 2008, **130**, 12787.

29 M. Toda, A. Takagaki, M. Okamura, J. N. Kondo, S. Hayashi, K. Domen and M. Hara, *Nature* 2005, **438**, 7065.

30 M. Hara, T. Yoshida, A. Takagaki, T. Takata, J. N. Kondo, S. Hayashi and K. Domen, *Angew. Chem. Int. Ed.* 2004, **43**, 2955.

31 P. A. Russo, M. M. Antunes, P. Neves, P. V. Wiper, E. Fazio, F. Neri, F. Barreca, L. Mafra, M. Pillinger, N. Pinna and A. A. Valente, *Green Chem.* 2014, **16**, 4292.

32 F. J. Liu, L. Wang, Q. Sun, L. F. Zhu, X. J. Meng and F.-S. Xiao, *J. Am. Chem. Soc.* 2012, **134**, 16948.

33 J. A. Melero, G. D. Stucky, R. van Griekena and G. Morales, *J. Mater. Chem.* 2002, **12**, 1664.

34 A. Zheng, S. J. Huang, S. B. Liu and F. Deng, *Phys. Chem. Chem. Phys.* 2011, **13**, 14889.

35 S. Pérez-Rodríguez, N. Rillo, M. J. Lázaro and E. Pastor, *App. Catal. B: Environ.* 2015, **163**, 83.

36 J. Wang, H. Y. Liu, J. Y. Diao, X. M. Gu, H. H. Wang, J. F. Rong, B. N. Zong and D. S. Su, *J. Mater. Chem. A* 2015, **3**, 2305.

37 R. Xu, W. Pang, J. Yu, Q. Huo and J. Chen, Chemistry of Zeolites and Related Porous Materials, Wiley, Singapore, 2007.

38 F. J. Liu, W. P. Kong, L. Wang, X. F. Yi, I. Noshadi, A. M. Zheng and C. Z. Qi, *Green Chem.* 2015, **17**, 480.

39 D. Margolese, J. A. Melero, S. C. Christiansen, B. F. Chmelka and G. D. Stucky, *Chem. Mater.* 2000, **12**, 2448.

40 Y. Chu, Z. Yu, A. Zheng, H. Fang, H. Zhang, S. J. Huang, S. B. Liu and F. Deng, *J. Phys. Chem. C* 2011, **115**, 7660.

41 M. D. Karra, K. J. Sutovich and K. T. Mueller, *J. Am. Chem. Soc.* 2002, **124**, 902.

42 F. de Clippel, M. Dusselier, R. V. Rompaey, P. Vanelderen, J. Dijkmans, E. Makshina, L. Giebeler, S. Oswald, G. V. Baron, J. F. M. Denayer, P. P. Pescarmona, P. A. Jacobs and B. F. Sels, *J. Am. Chem. Soc.* 2012, **134**, 10089.

43 E. Nikolla, Y. Román-Leshkov, M. Moliner and M. E. Davis, *ACS Catal.* 2011, **1**, 408.

44 L. Wang, H. Wang, F. J. Liu, A. M. Zheng, J. Zhang, Q. Sun, J. P. Lewis, L. F. Zhu, X. J. Meng and F.-S. Xiao, *ChemSusChem* 2014, **7**, 402.

45 R. J. van Putten, J. C. van der Waal, E. de Jong, C. B. Rasrendra, H. J. Heeres and J. G. de Vries, *Chem. Rev.* 2013, **113**, 1499.

Table 1 Structural parameters, and acid concentrations of various solid acids.

Run	Samples	S_{BET} [a]	D_p [b]	V_p [a]	S content [c]	Acid
n		(m^2/g)	(nm)	(cm^3/g)	(mmol/g)	concentrations [d] (mmol/g)
1	NPC	1600	0.63	0.82	-	-
2	NPC-[C_3N][SO_3CF_3]	525	4.0	0.36	2.1	2.35
3	NPC-[C_3N][SO_4H]	510	3.4	0.33	2.3	2.5
4	NPC-[C_3N][$H_2PW_{12}O_{40}$]	168	2.2	0.13	1.3	2.1
5	Amberlyst 15	45	40.0	0.31	4.30	4.70
6	SBA-15-SO_3H	820	7.3	1.40	1.26	1.36
7	H-ZSM-5 [e]	364	0.55	0.16	-	0.40
8	H-USY [f]	623	14.7	0.26	-	1.8

[a] The data was obtained from N_2 adsorption results.

[b] The mesopore size (>2 nm) distribution was calculated using BJH model, the micropore size distribution (1.0 nm <) was calculated using Horvath-Kawazoe model.

[c] The data was obtained from elemental analysis results.

[b] The data was obtained from acid-base titration.

[e] Si/Al ratio at 40.

[f] Si/Al ratio at 7.5.

Table 2 Transformation of fructose into HMF and furan-2,5-dicarbaldehyde catalyzed by various solid acids. The yield of HMF was analyzed by liquid chromatography (SHIMADZU, LC-20A) based on standard curve method, and the major by-products were LA, FA and some others.

Run	Catalysts	Furan-2,5-dicarbaldehyde yield (%) [a]	HMF yield (%) [a]	By-products (%)
1	NPC-[C_3N][SO_3CF_3]	8.1	79.5	3.7
2	SBA-15-SO_3H	4.1	53.2	1.2
3	H-form ZSM-5	3.7	38.6	Trace
4	Amberlyst-15	4.6	50.3	2.3
5	NPC-[C_3N][SO_4H]	7.8	80.1	4.1
6	NPC-[C_3N][SO_3CF_3] [b]	7.5	77.2	3.4

[a] Analyzed by using HPLC system based on standard curves method.

[b] Fifth run to test reusability of the catalyst.

Table 3 Yields of sugars and dehydration products in the depolymerization of Avicel catalyzed by various solid acids.

Run	Catalysts	Glucose yield (%) [a]	Cellobiose yield (%) [a]	HMF yield (%) [a]	TRS (%) [b]
1	Amberlyst 15	30.3	18.4	4.6	60.2
2	H-ZSM-5	10.4	7.6	2.8	26.7
3	SBA-15-SO_3H	25.4	13.6	4.1	51.8
4	H-USY	22.5	11.2	3.5	42.6
5	NPC-[C_3N][SO_3CF_3]	50.3	17.3	9.8	78.5
7	NPC-[C_3N][SO_4H]	47.5	22.3	9.2	79.2

[a] Measured by HPLC method, the reaction time was 5 h. [b] Yields of TRS were measured by DNS method.

Table 4 Catalyze synthesis of bisphenol-A over various solid acids.

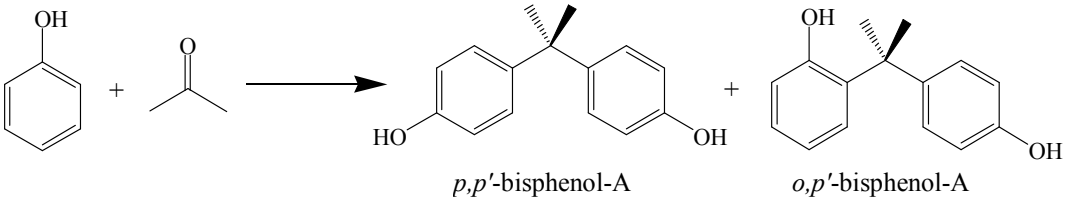

p,p′-bisphenol-A *o,p′*-bisphenol-A

Run	Samples	Phenol conversion (%)	TOF (h^{-1}) [a]	*p,p′*/*o,p′* molar ratio
1	Amberlyst 15	13.4	1.2	9.6
2	H-ZSM-5	4.8	5.0	8.7
3	H-USY	8.7	2.0	8.9
4	SBA-15-SO_3H	10.9	3.3	9.4
5	NPC-[C_3N][SO_3CF_3]	21.4	3.8	9.8
6	NPC-[C_3N][SO_4H]	22.5	3.75	10.1
7	NPC-[C_3N][$H_2PW_{12}O_{40}$]	20.6	4.1	9.4

[a] TOF is based on mmol of phenol per mmol of active site.

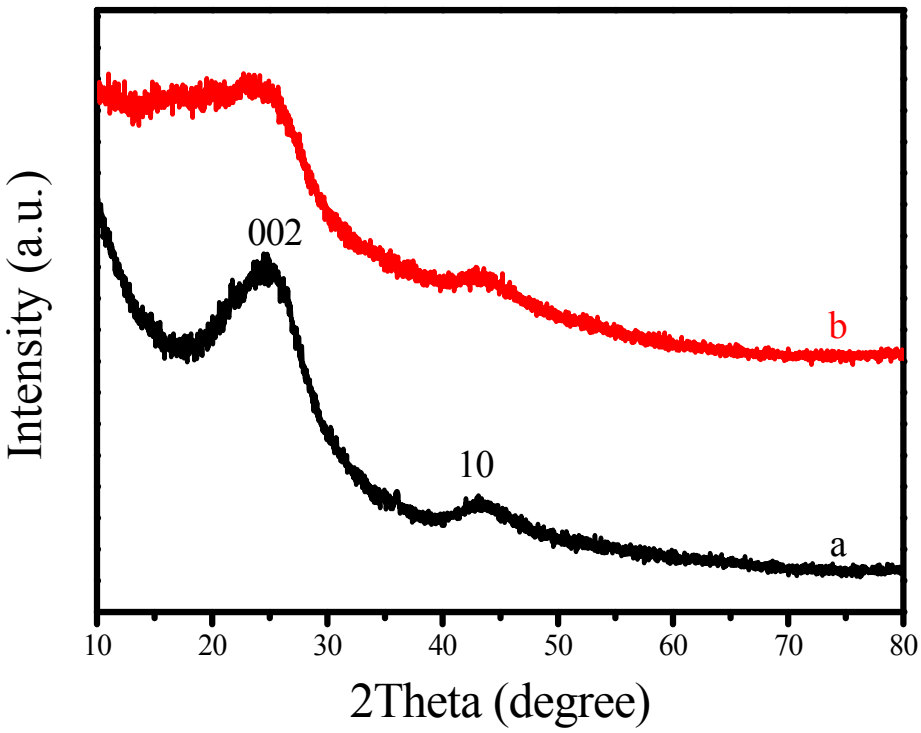

Figure 1 XRD patterns of (a) NPC and (b) NPC-$[C_3N][SO_3CF_3]$.

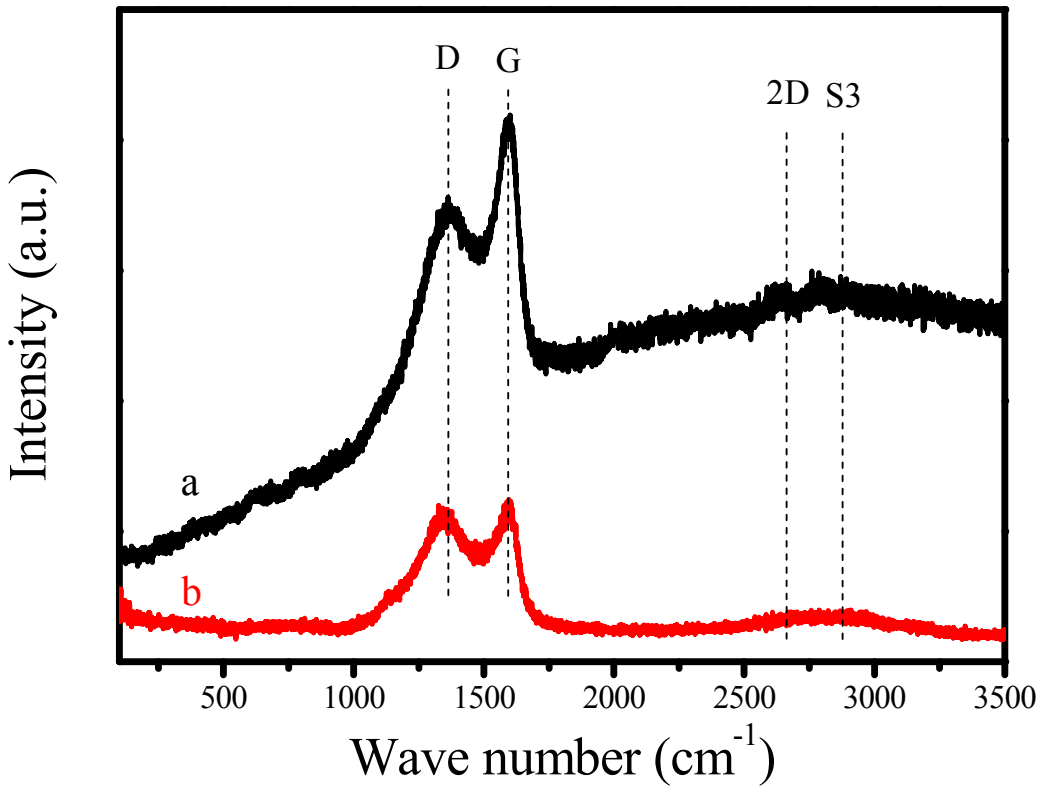

Figure 2 Raman spectra of (a) NPC and (b) NPC-$[C_3N][SO_3CF_3]$.

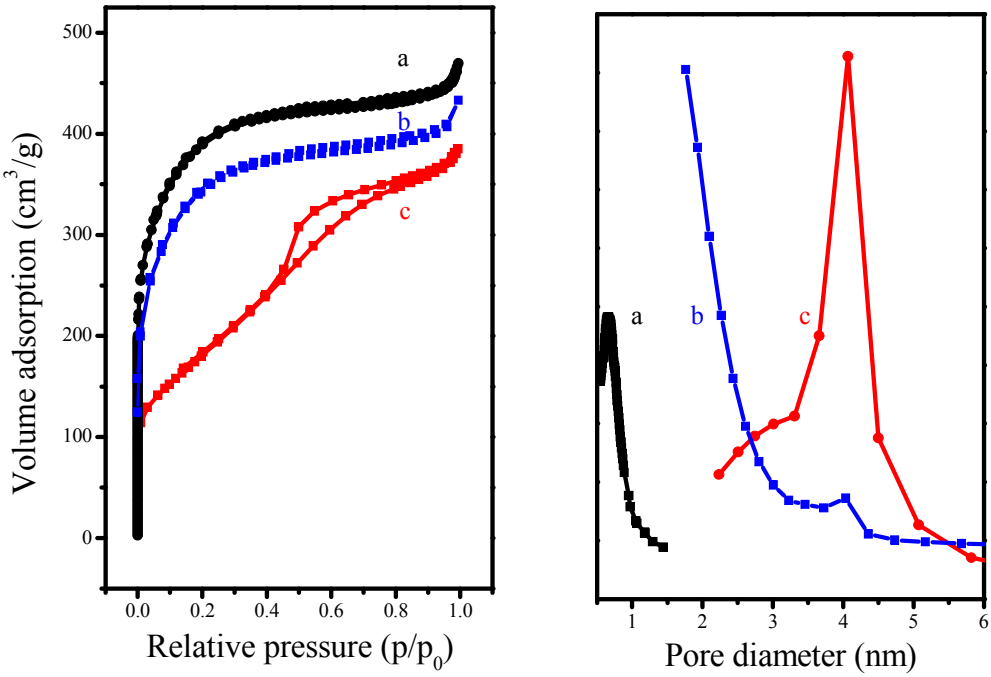

Figure 3 N_2 isotherms and pore size distribution of (a) NPC and (b) NPC-$[C_3N]^+$ and (c) NPC-$[C_3N][SO_3CF_3]$.

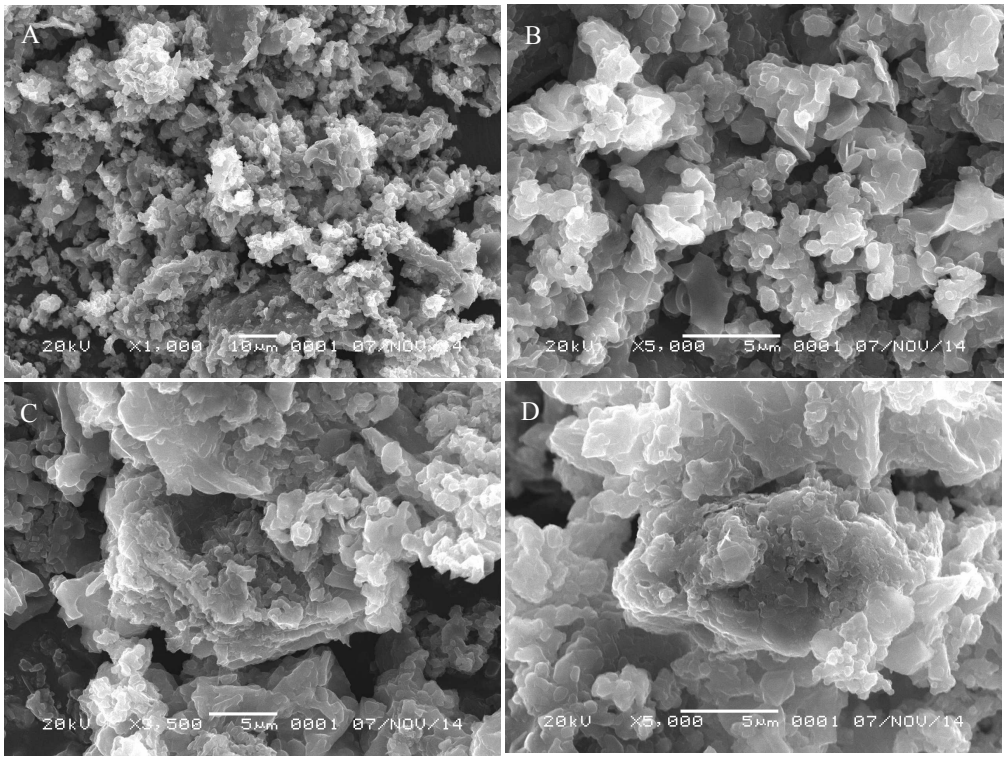

Figure 4 SEM images of NPC-$[C_3N][SO_3CF_3]$.

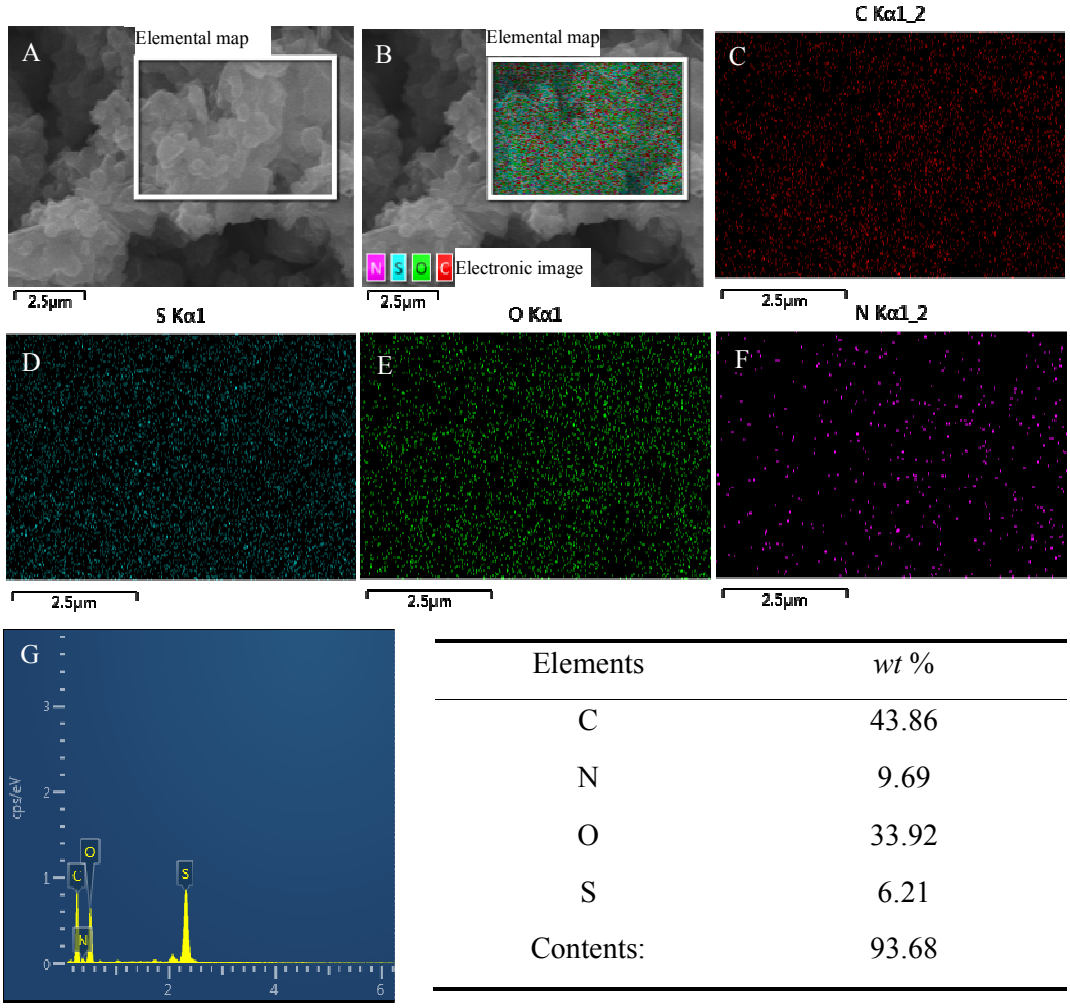

Elements	*wt* %
C	43.86
N	9.69
O	33.92
S	6.21
Contents:	93.68

Figure 5 Elemental maps, EDX spectrum and element contents of various elements in NPC-$[C_3N][SO_3CF_3]$.

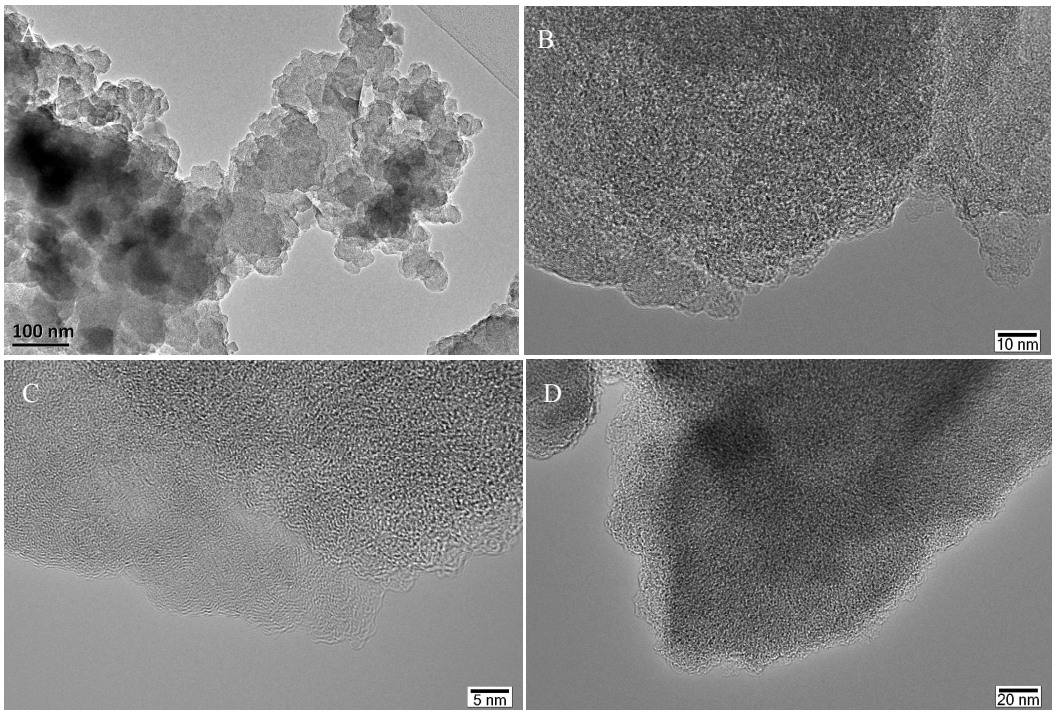

Figure 6 TEM images of NPC-[C_3N][SO_3CF_3].

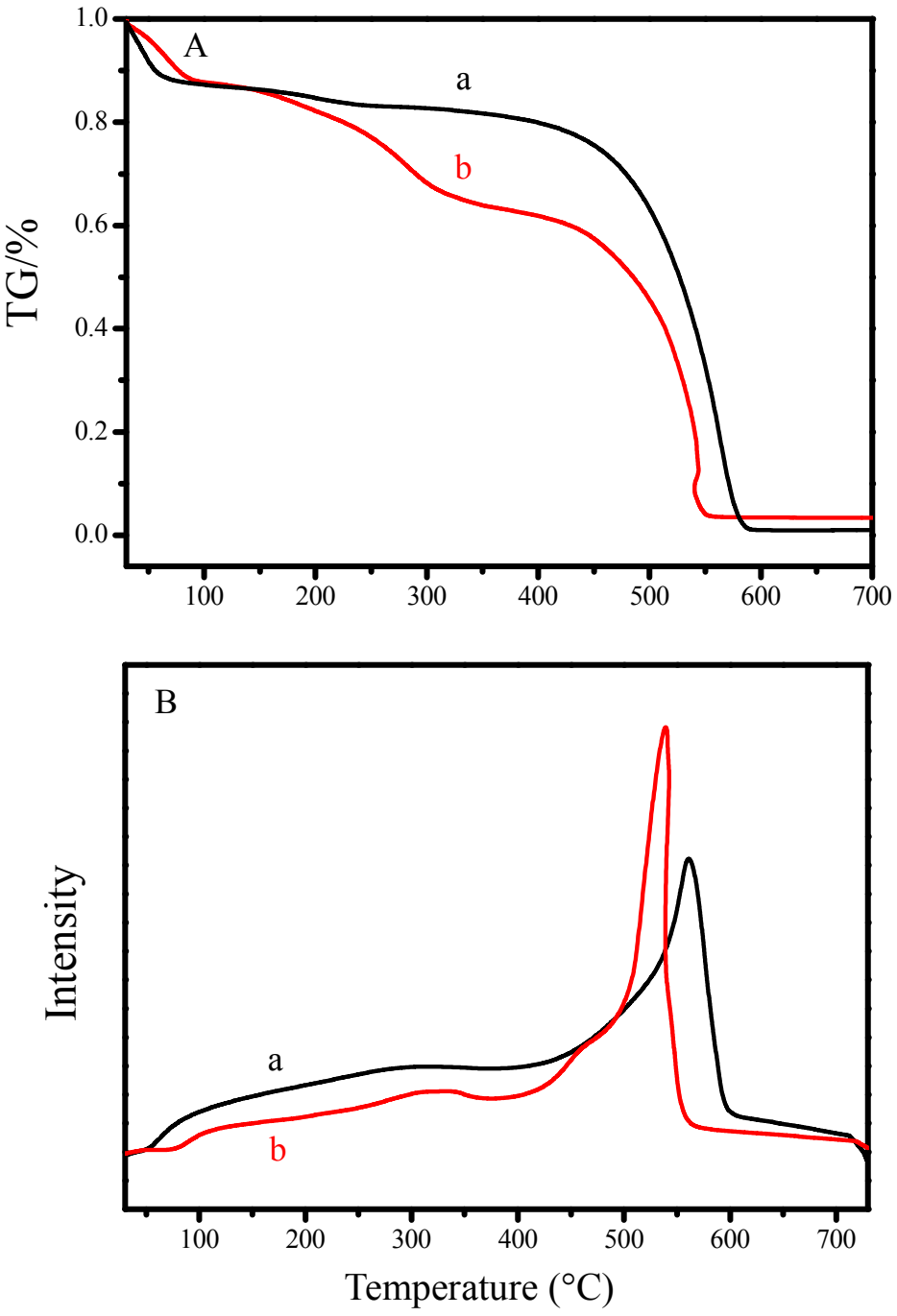

Figure 7 (A) TG and (B) DTA curves of (a) NPC and (b) NPC-$[C_3N][SO_3CF_3]$.

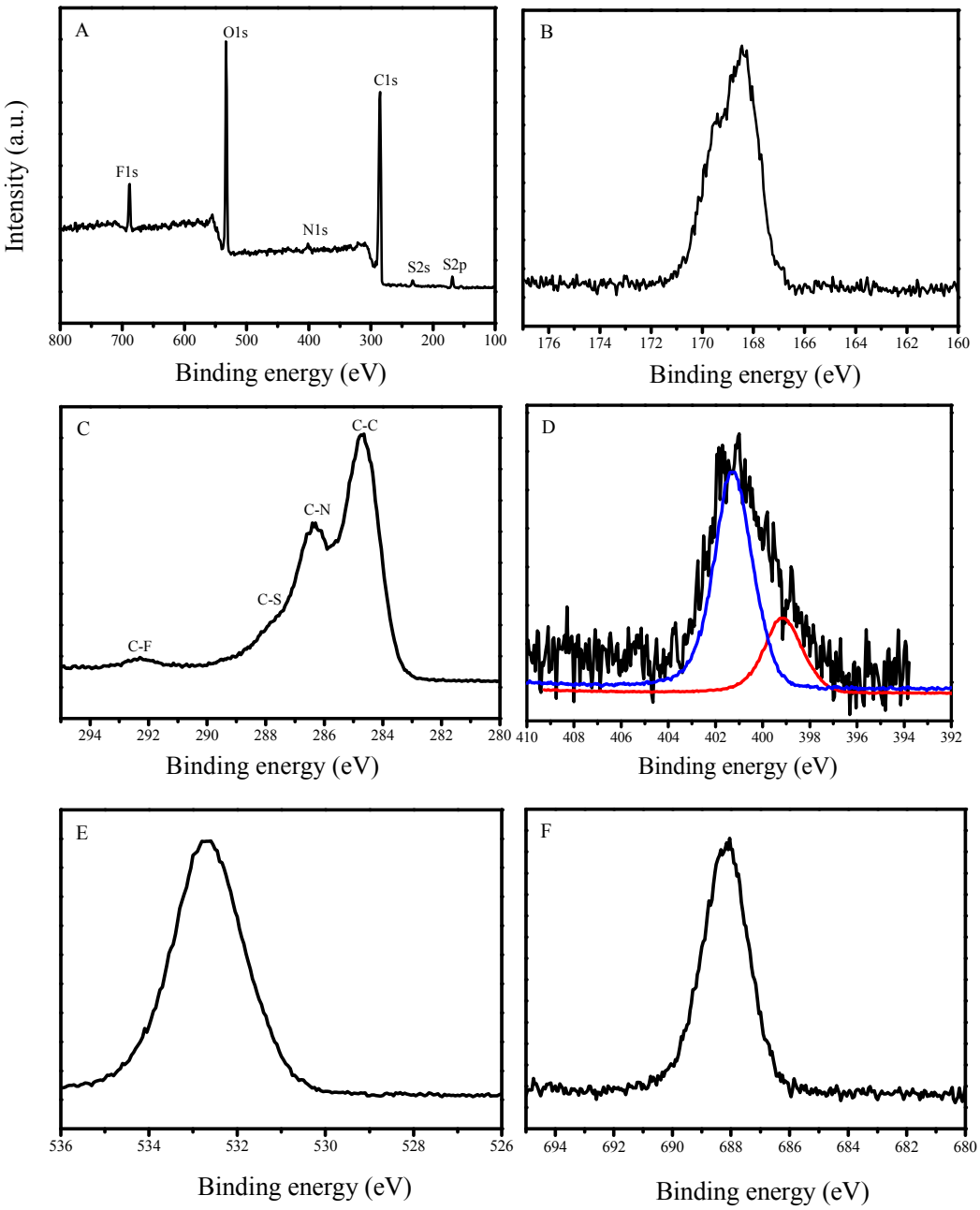

Figure 8 XPS spectra of (A) survey, (B) S2p, (C) C1s, (D) N1s, (E) O1s and (F) F1s of NPC-[C_3N][SO_3CF_3].

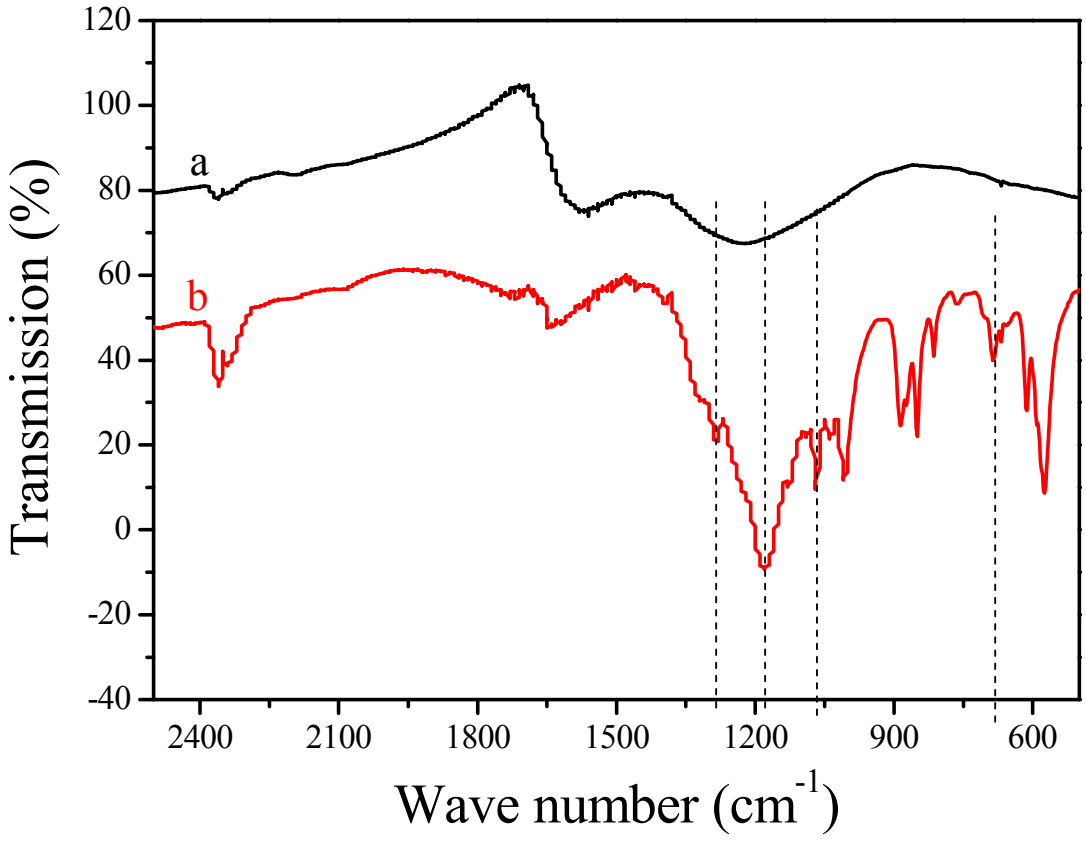

Figure 9 FT-IR spectra of (a) NPC and (b) NPC-$[C_3N][SO_3CF_3]$.

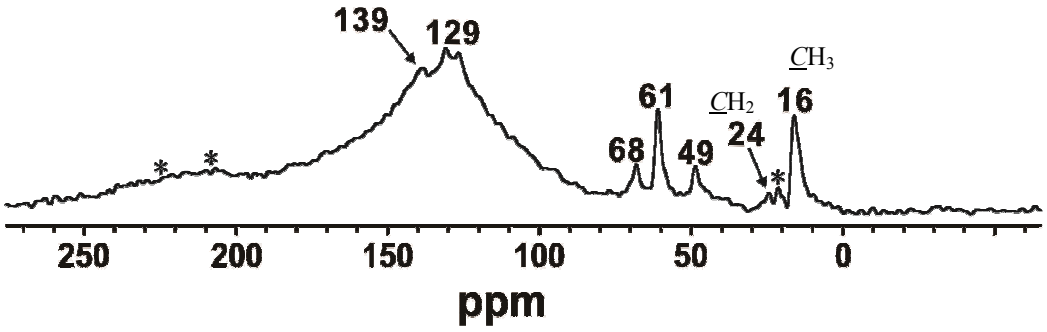

Figure 10 ^{13}C solid NMR spectrum of NPC-$[C_3N][SO_3CF_3]$.

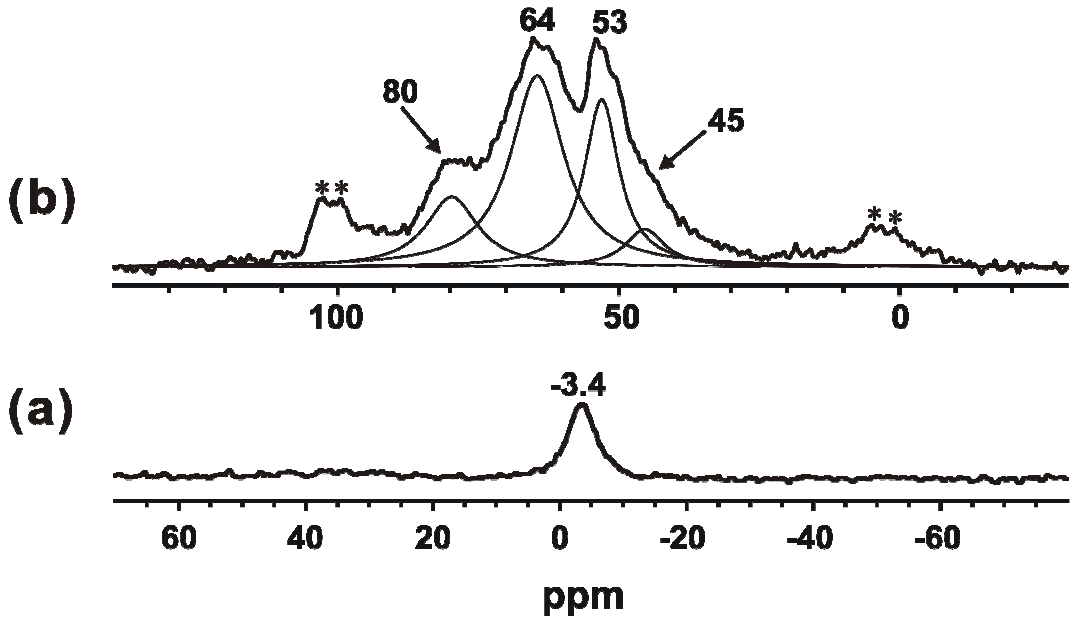

Figure 11 Room temperature ^{31}P MAS NMR spectra of adsorbed (a) TMP acquired with proton decoupling, and (b) TMPO of NPC-$[C_3N][SO_3CF_3]$.

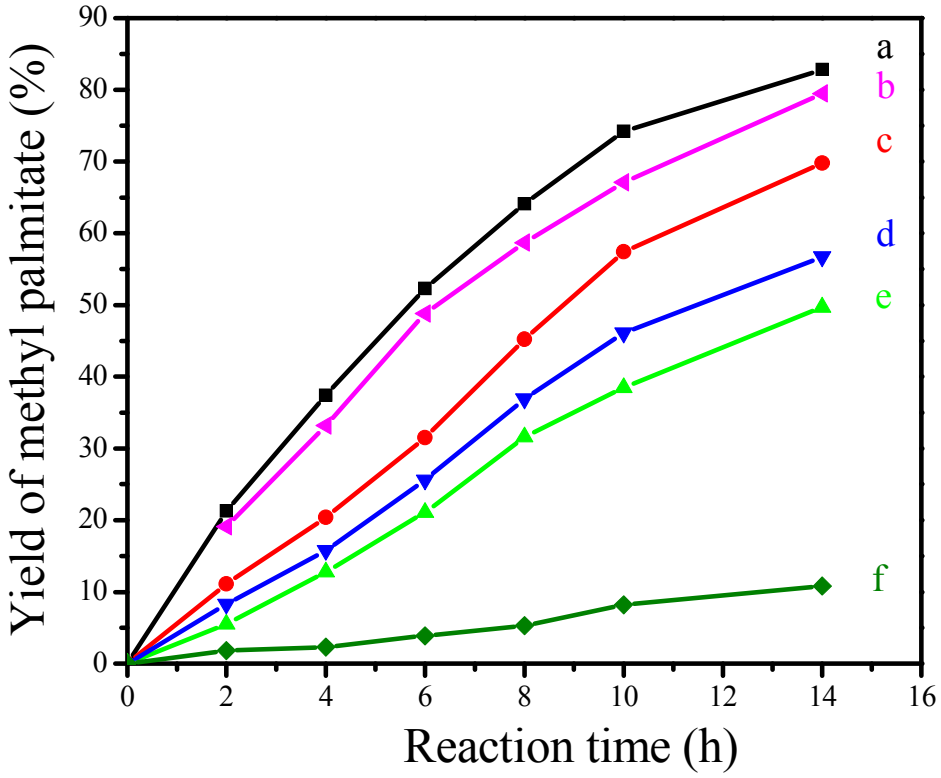

Figure 12 Catalytic kinetics curves in transesterification of tripalmitin with methanol over by (a) NPC-$[C_3N][SO_3CF_3]$, (b) 5^{th} recycled NPC-$[C_3N][SO_3CF_3]$, (c) $H_3PW_{12}O_{40}$, (d) SBA-15-SO_3H, (e) Amberlyst 15 and (f) H-form ZSM-5 zeolite.

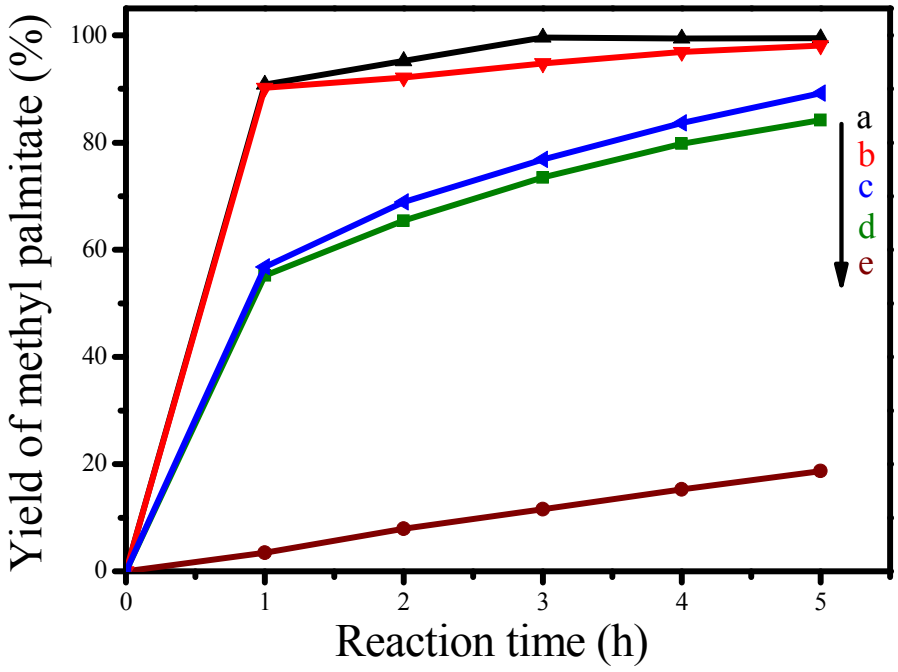

Figure 13 Dependence of product yields on reaction time in esterification of palmitic acid with methanol over by (a) NPC-$[C_3N][SO_3CF_3]$, (b) $H_3PW_{12}O_{40}$, (c) SBA-15-SO_3H, (d) Amberlyst 15 and (e) H-form ZSM-5 zeolite.

Graphical abstract

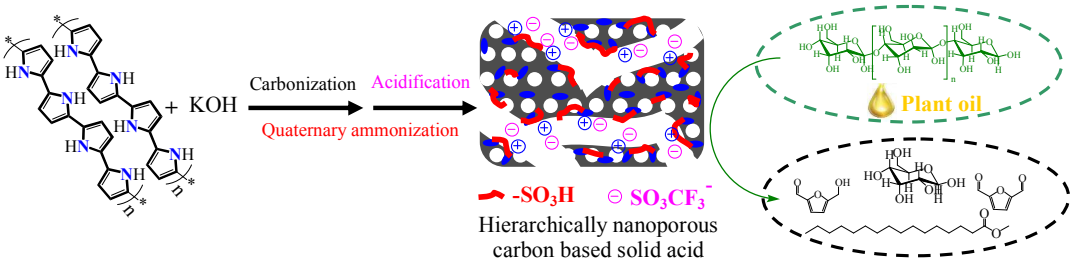

Highly porous carbonaceous solid acids with large BET surface areas, controllable and strong acidity, and enhanced performances for catalyzing production of useful chemicals and biofuels have been successfully synthesized under template free conditions.